

## Iron Electrodeposition in a Magnetic Field

Hisayoshi Matsushima<sup>1,\*</sup>, Yasuhiro Fukunaka<sup>2</sup>, Shiomi Kikuchi<sup>3</sup>, Adriana Ispas<sup>4</sup> and Andreas Bund<sup>4</sup>

<sup>1</sup> Interdisciplinary Graduate School of Medicine and Engineering, University of Yamanashi, 4-3-11 Takeda, Kofu 400-8511, Japan.

<sup>2</sup> Graduate School of Energy Science, Kyoto University, Sakyo-ku, Kyoto 606-8501, Japan

<sup>3</sup> Department of Material Science, University of Shiga Prefecture, Shiga 522-2500, Japan.

<sup>4</sup> Institute of Physical Chemistry & Electrochemistry, Technical University of Dresden, D-01062 Dresden, Germany.

\*E-mail: [hisayoshim@yamanashi.ac.jp](mailto:hisayoshim@yamanashi.ac.jp)

Received: 6 August 2012 / Accepted: 30 August 2012 / Published: 1 October 2012

---

Iron was electrodeposited in the sulfuric acid solution and a magnetic field was superimposed parallel to the electrode surface. The iron current efficiency calculated by the gravimetric analysis suggested that the hydrogen gas evolution was more promoted with increasing the magnetic field intensity. This was explained by the magnetohydrodynamic (MHD) convection stirring the electrolyte solution in the vicinity of the electrode surface. The convective effect could reduce the thickness of the H<sup>+</sup> diffusion layer, resulting in the enhancement of the H<sup>+</sup> mass transfer toward the electrode. XRD pattern in no magnetic field demonstrated that the crystal structure was random orientation at the beginning of the deposition, but later (211) plane was preferentially selected more with increasing the film thickness. Three dimensional XRD analysis by pole figure measurement showed that the (110) plane was orientated in the direction of the magnetic field at 30 degrees normal to the electrode surface. The high magnetic field accelerated the formation rate of the (110) plane orientation.

---

**Keywords:** MHD; Electrodeposition; Iron; Hydrogen Evolution, Crystal Orientation; Magnetic Field

### 1. INTRODUCTION

“Magneto-electrochemistry” has attracted many attentions due to the unique environment as a degree of new freedom for the electrochemical reaction [1-13]. It is very interesting if the magnetic field (B) influences the kinetic factors controlled by the electron transfer [14, 15]. However it is difficult to distinguish the influence of B on the kinetic factors because some multiple factors are co-existed in B.

The magnetohydrodynamic (MHD) effect is well known. When an electrical field is applied vertical to a magnetic field, the MHD convection in an electrolytic solution is induced by the electromagnetic interaction. The MHD flow is directly estimated by simulation [16-18] and visualized by some indicators [19, 20]. The MHD effect can be indirectly confirmed by observing the surface morphology and the crystal orientation of the electrodeposited films [21-25]. It has been usually reported that the surface roughness becomes smoother with increasing B intensity. This is explained by the mass transfer enhancement by MHD convection, as the relation between the concentration and the morphology is known as *coupling phenomena* [26]. Thus, it stirs the electrolyte solution in the vicinity of the electrode surface and then helps uniformly forming the concentration boundary layer, leading to the thinner diffusion layer.

Concerning on the crystal orientation, Devos et al. [27, 28] reported that a magnetic field could change the preferred orientation of the nickel grain due to the increase of the diffusion flux of definite inhibiting species. In our previous study [29], the crystal orientation in the growth direction of the deposited film was controlled by the electrochemical factor, but the pole figure measurement demonstrated the newly formed crystal orientation in the B direction. Thus the iron crystal grows with the uni-axial mode in no B, while it obeys the biaxial one in B. However the mechanism is so complicated that the reason is still unclear.

The study of the transient process during the electrodeposition in B can give the new information for considering the growth mechanism. In this paper, the iron electrodeposition is galvanostatically carried out in B and the transient variations of the electrode potential, current efficiency and the crystal orientation are investigated.

## 2. EXPERIMENTAL

The electrodeposition apparatus and method have been described in our previous paper [29]. Thus, only several important points are described here.

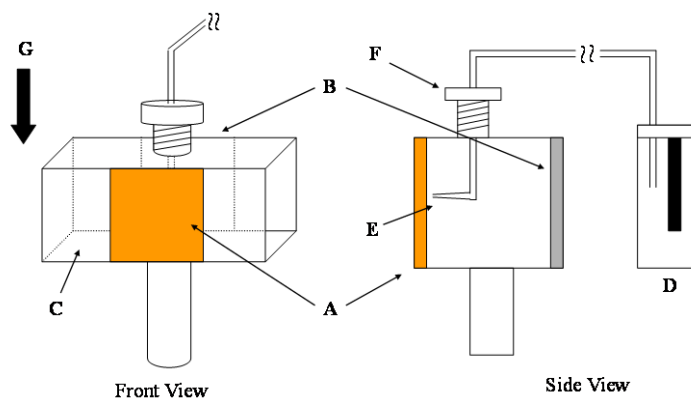


**Figure 1.** Schematic illustration of the electrode assembly. A: Cathode ( $\text{Cu}$ ,  $1 \text{ cm}^2$ ), B: Anode ( $\text{Fe}$ ,  $1 \text{ cm}^2$ ), C: Channel ( $10 \text{ mm} \times 10 \text{ mm} \times 30 \text{ mm}$ ), D: Reference ( $\text{Ag} / \text{AgCl}$ ), E: Luggin probe, F: Plastic screw, G: Magnetic flux.

Electrochemical experiments were carried out with a three-electrode system as illustrated in Fig. 1. The cathode was a sheet of copper (10 mm x 10 mm x 0.2 mm, Cu 99.99 %, Nilaco Corp.). The anode was a sheet of pure iron (10 mm x 10 mm x 0.2 mm, Fe 99.99 %, Nilaco Corp.). A reference electrode was an Ag / AgCl electrode with a saturated KCl (3.33 mol l<sup>-1</sup>) aqueous solution.

An electrolyte composition was 0.90 mol l<sup>-1</sup> FeSO<sub>4</sub> · 7 H<sub>2</sub>O, 0.15 mol l<sup>-1</sup> FeCl<sub>2</sub> · 4 H<sub>2</sub>O and 0.43 mol l<sup>-1</sup> NH<sub>4</sub>Cl. The pH of the electrolyte was adjusted to 1.5 with H<sub>2</sub>SO<sub>4</sub>. It was deaerated by bubbling argon gas for more than an hour. The solution temperature was maintained at 298 K.

The iron electrodeposition was conducted galvanostatically at 10 mA cm<sup>-2</sup> by the amount of electrical charge reached 150 C cm<sup>-2</sup>. A static and uniform magnetic field was superimposed parallel to the electrode surface with magnitude up to 5 T, The magnetic field was generated by a helium free resistive magnet (CSM-6T, Sumitomo Heavy Industries).

The weight of each sample was measured in order to estimate a current efficiency for the iron electrodeposition. The preferred crystal orientation was measured by XRD using Cu-K $\alpha$  line (Multiflex, Rigaku, 40 kV, 40 mA; X'Pert, Philips, 50 kV, 40 mA).

### 3. RESULTS AND DISCUSSION

The electrolyte containing Fe<sup>2+</sup> ion was easily oxidized during the long time experiment to produce the finer particles as an impurity.

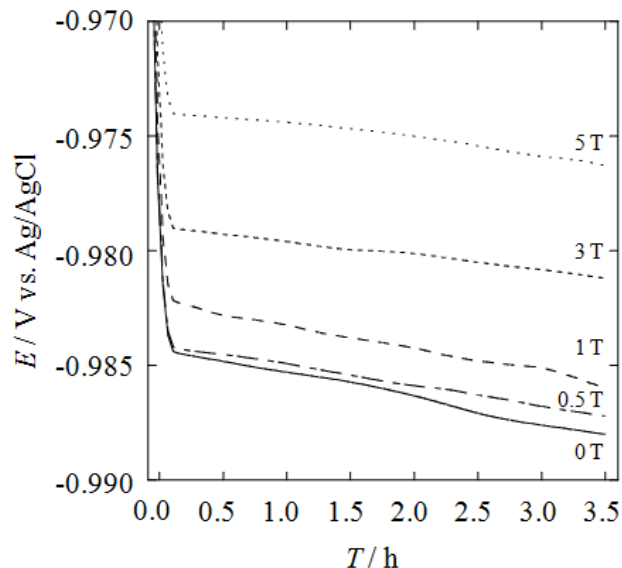


**Figure 2.** The potential-time curves during iron electrodeposition at 10 mA cm<sup>-1</sup> in various of the B intensities at 298 K.

Therefore the iron electrodeposition was carried out in N<sub>2</sub> atmosphere in order to keep the steady deposition condition. The iron deposition potential was measured and the potential-time curves were shown in Fig. 2. The sampling interval was 1 minute. The deposition potential reached the

constant value around - 0.98 V, as soon as the measurement was started. But the potential value clearly depended on the magnetic field. It shifted toward more anodic direction with increasing in the B intensity. For example, it changed from - 0.985 V vs. Ag/AgCl at 0 T to -0.975 V at 5 T. The potential difference is probably caused by the ohmic resistance rather than the kinetic factor. The rest potential relating to the equilibrium state of the iron electrodeposition/dissolution reaction has been reported to be unchanged in a high magnetic field [30]. Probably the magnetic field energy is not as large as that of the electric field. Therefore the electrochemical reaction controlled by the charge transfer is hardly influenced by the magnetic field. On the other hand, MHD convection generated in a magnetic field can remove the hydrogen gas bubble sticking the electrode surface [19] and reduce the void fraction of the electrolyte between the working and reference one [19, 31]. The present result demonstrates that the MHD convection can actively pump the solution as well as the natural convection induced by the uprising gas bubbles.

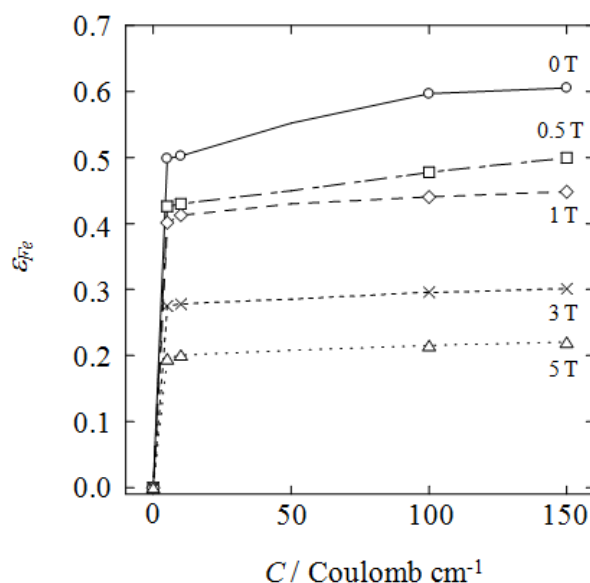


**Figure 3.** The iron current efficiency calculated from the weight of the iron film electrodeposited at several deposition time (electric coulomb number) in various of the B intensities.

The iron current efficiency,  $\epsilon_{\text{Fe}}$ , was calculated from the weight of iron deposits. The sample film was collected and the weight was measured when the electric coulomb reached 5, 10, 50, 100, 150 C cm<sup>-1</sup>, respectively. The superimposition of the magnetic field remarkably caused the reduction of  $\epsilon_{\text{Fe}}$ . It decreased from 0.5 at 0 T to 0.2 at 5 T, as seen in Fig. 3. The reason why the hydrogen evolution was accelerated by a magnetic field might be explained by the mass transfer. The hydrogen evolution is assumedly controlled by the mass transfer rather than the electric charge transfer, because the applied potential was much more cathodic (around - 0.9 V vs. Ag/AgCl) than the hydrogen evolution potential (-0.22 V vs. Ag/AgCl). The MHD convection enhances the mass transfer of both reaction species of H<sup>+</sup> and Fe<sup>2+</sup> in B. Thus, it reduces the concentration layer of H<sup>+</sup>, resulting in the increase of

$H^+$  mass flux to the electrode surface. On the other hand, the iron deposition has not yet to reach the mass transfer limitation due to the high concentration of  $0.9 \text{ mol L}^{-1}$ .

The rate of iron deposition slightly increased depending on the deposition time. It increased from  $0.52$  at  $5 \text{ C cm}^{-1}$  to  $0.61$  at  $150 \text{ C cm}^{-1}$  in no magnetic field, while the difference in  $5 \text{ T}$  was hardly confirmed. This might be attributed to the hydroxide formation on the electrode surface. In lower  $B$  intensities where the MHD convection is too slow to stir the electrolyte in the vicinity of the electrode, the surface pH is shifted toward the higher value by the mass transfer limitation of  $H^+$ . The surface pH locally reaches enough high to form the iron hydroxide which is inactive site for the hydrogen evolution reaction.

The electrodeposited film forms the crystal orientation in the direction of the film growth (normal to the electrode surface). The several factors such as the overpotential, the film strain and the surface concentration are considered. The degree of the crystal orientation is defined as crystal orientation,  $M$ , by comparing the power pattern without any orientation states (random mode). It is calculated as follows,

$$M(hkl) = \frac{\frac{I(hkl)}{\sum I(hkl)}}{\frac{I_0(hkl)}{\sum I_0(hkl)}} \quad (1)$$

where  $M(hkl)$  is the orientation index,  $I(hkl)$  is peak intensity and  $\sum I$  is the sum of intensities of the three independent peaks: (110), (211), (222). The index 0 in  $I_0(hkl)$  refers to the intensities of powder pattern given in JCPDS card.

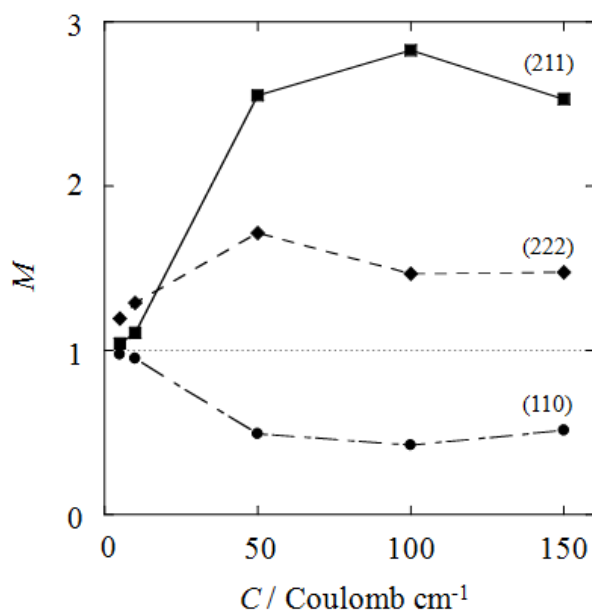


**Figure 4.** Dependence of orientation index,  $M$ , on the coulomb number for the iron films electrodeposited in no magnetic field. ●: (110) plane, ■: (211) plane and ◆: (222) plane.

Figure 4 shows the transient behavior of  $M$  depending on the deposition time. The figure demonstrates the result in no magnetic field. The film did not clearly form the preferential crystal orientation until the deposition electric charges reached the  $10 \text{ C cm}^{-1}$ . The crystal plane of (211) and (222) were selected, while the growth of (110) plane was inhibited. The crystal selection was completed by  $50 \text{ C cm}^{-1}$  and then the crystal orientation of (211) was dominated independently of the deposition time.

In order to investigate the three dimensional crystal orientation, X-ray pole figure measurements were conducted for the iron films electrodeposited at 10, 100 and  $150 \text{ C cm}^{-1}$ . The pole figure can reveal crystal orientation not seen in Theta-2 Theta diffractometer. The figure is plotted in polar coordinates consisting of the tilt and rotation angles with respect to a given crystallographic orientation.

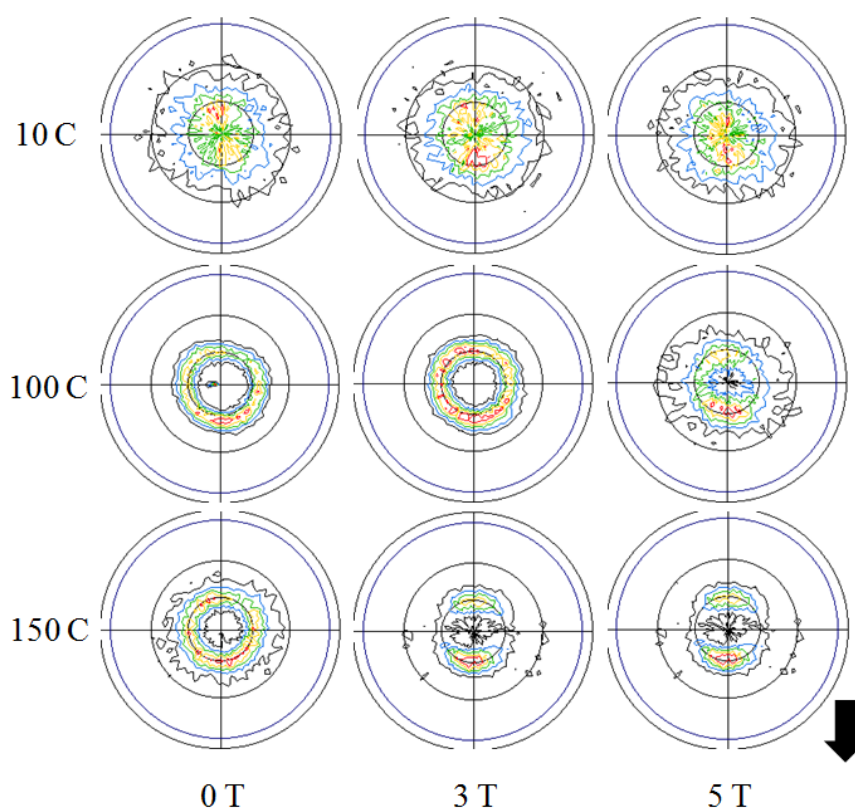


**Figure 5.** Pole figures of iron (110) plane electrodeposited at several electric coulomb number (10, 100,  $150 \text{ C cm}^{-1}$ ) and B intensities (0, 3, 5 T). An arrow shows magnetic field direction.

Figure 5 shows pole figures of iron (110) plane electrodeposited in 0, 3 and 5 T, respectively. The magnetic field was applied parallel to the substrate surface and its direction is indicated by an arrow in Fig. 5. The high intensity area (surrounded by red and yellow lines) with broad band was observed at  $10 \text{ C cm}^{-1}$ , independently of B. It slightly formed the anisotropic pattern at the angle between 0 and 30 degrees to the direction normal to the substrate plane. Thus, the asymmetric crystal orientation in a plane is formed by the substrate effect, because the thickness of iron deposits is so thin ( $\sim$  a few  $\mu\text{m}$ ) that the iron crystal structure is followed by the copper crystal texture.

The pattern broadly concentrated at the center at  $5 \text{ C cm}^{-1}$  changed the circle one at the angle of 30 degree at 0 and 3 T, as the deposition proceeded until  $100 \text{ C cm}^{-1}$ . This circle pattern indicates that (110) planes face arbitrary directions randomly. The iron film could be grown without any influences of the substrate. In high magnetic field of 5 T, there was an obvious crystal orientation in same direction of the magnetic field vector. It was more clearly observed with increasing the film thickness, as seen in  $150 \text{ C cm}^{-1}$ . The same anisotropic pattern appeared at 3 T at  $150 \text{ C cm}^{-1}$ , after detecting the circle pattern as well as in 0 T at  $100 \text{ C cm}^{-1}$ . This transient behavior indicates that the crystal orientation in the plane is not influenced by the substrate texture.

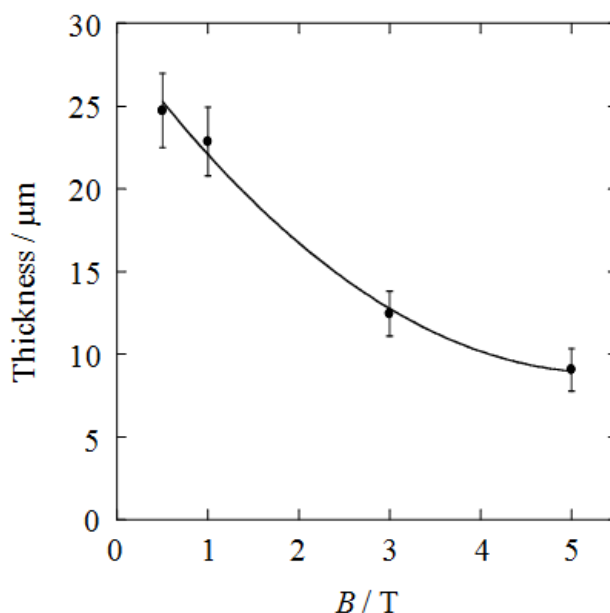


**Figure 6.** The onset of the film thickness at which the anisotropic pattern was formed in various of the B intensities.

The film thickness at which the anisotropic pattern is observed by the pole figure is plotted in Fig. 6. Supposed that the iron was uniformly electrodeposited, the thickness was calculated by the current efficiency (Fig. 3). The crystal orientation of (110) plane was observed at more than a few  $\mu\text{m}$  in all cases. The enough thickness supported again that the texture of (110) plane was hardly controlled by the substrate structure. The selection process of (110) orientation was depended on the B intensity. The competition among some crystal planes was completed more quickly with increasing the B intensity.

The crystal orientation of the transient metal electrodeposition accompanied with hydrogen evolution, in the present case, is probably influenced by surface pH, as discussed in Fig. 3. The hydrogen evolution consumption causes so high pH value that the hydroxides and other iron oxides can be produced on the surface. The formation of the hydroxides is inhibited and the atomic hydrogen is more generated on the lateral surface facing MHD direction because the mass flux of  $\text{H}^+$  ion is enlarged. Li and Szpunar demonstrated that the surface energy anisotropy was influenced by the co-

deposition of hydrogen and explained the texture variation depending on the electrodeposition condition [32]. The present results in B could be attributed to the surface anisotropic energy depended on MHD direction.

#### 4. SUMMARY

Transient behaviors of the current efficiency and the crystal orientation of the iron film galvanostatically electrodeposited in B were measured. The enhancement of  $H^+$  mass transfer by MHD convection slowed the rate of the film growth with increasing B intensity. The film hardly formed the crystal orientation initially and then the crystal plane normal to the electrode surface (the growth direction) was mainly dominated by the (211) plane with increasing the film thickness. The pole figure measurement of (220) plane demonstrated that the crystal growth mechanism in B followed three steps, i) random, ii) uniaxial and iii) biaxial mode, depending on the film thickness. The formation of biaxial mode was more quickly with increasing B intensity.

#### References

1. T. Z. Fahidy, *Progress in Surface Science* 68 (2001) 155
2. R. A. Tacke and L. J. J. Janssen, *J. Appl. Electrochem.*, 25 (1995) 1
3. S. Mohan, G. Saravanan, A. Bund, *Electrochim. Acta*, 64 (2012) 94
4. R. Sueptitz, K. Tschulik, M. Uhlemann, L. Schultz and A. Gebert, *Electrochim. Acta*, 56, (2012) 5866
5. A. Ispas, H. Matsushima, A. Bund and B. Bozzini, *J. Electroanal. Chem.*, 651 (2011) 197
6. D. Fernandez, Z. Diao, P. Dunne and J. M. D. Coey, *Electrochim. Acta*, 55 (2010) 8664
7. G. Mutschke, K. Tschulik, T. Weier, M. Uhlemann, A. Bund and J. Frohlich, *Electrochim. Acta*, 55 (2010) 9060
8. A. Ispas, H. Matsushima, A. Bund and B. Bozzini, *J. Electroanal. Chem.*, 626 (2009) 174
9. A. Ispas, H. Matsushima, W. Plieth and A. Bund, *Electrochim. Acta*, 52 (2007) 2785
10. K. L. Rabah, J. P. Chopart, H. Schloerb, S. Saulnier, O. Aaboubi, M. Uhlemann, D. Elmi and J. Amblard, *J. Electroanal. Chem.*, 571 (2004) 85
11. C. O'Reilly, G. Hinds and J. M. D. Coey, *J. Electrochem. Soc.*, 148 (2001) C674
12. R. N. Brien and K. S. V. Santhanam, *J. Appl. Electrochem.*, 27 (1997) 573
13. J. P. Chopart, J. Douglade, P. Fricoteaux and A. Olivier, *Electrochim. Acta*, 36 (1991) 459
14. F. M. F. Rhen, G. Hinds and J. M. D. Coey, *Electrochem. Commun.*, 6 (2004) 413
15. O. Devos, O. Aaboubi, J. P. Chopart, A. Olivier, C. Gabrielli and B. Tribollet, *J. Phys. Chem. A*, 104 (2000) 1544
16. D. Sen, K. M. Isaac, N. Leventis and I Fritsch, *Int. J. Heat Mass Transf.*, 54 (2011) 5368
17. G. Mutschke, A. Hess, A. Bund and J. Froehlich, *Electrochim. Acta*, 55 (2010) 1543
18. G. B. N. Boum and A. Alemany, *Electrochim. Acta*, 44 (1999) 1749
19. H. Matsushima, T. Iida and Y. Fukunaka, *J. Solid State Electrochem.*, 16 (2012) 617
20. X. G. Yang, K. Eckert, K. Seidel and M. Uhlemann, *Electrochim. Acta* 54 (2008) 352
21. J. Koza, M. Uhlemann, A. Gebert, L. Schultz and J. Ludwig, *J. Solid State Electrochem.* 12 (2008) 181
22. H. Matsushima, A. Bund, W. Plieth, S. Kikuchi and Y. Fukunaka, *Electrochim. Acta*, 53 (2007) 161-166
23. H. Matsushima, Y. Fukunaka, Y. Ito, A. Bund and W. Plieth, *J. Electroanal. Chem.*, 587 (2006) 93

24. M. Motoyama, Y. Fukunaka and S. Kikuchi, *Electrochim. Acta*, 51 (2005) 897
25. A. Bund and A. Ispas, *J. Electroanal. Chem.*, 575 (2005) 221
26. Y. Fukunaka, K. Denpo, M. Iwata, K. Maruoka and Y. Kondo, *J. Electrochem. Soc.* 130 (1983) 2492
27. O. Devos, A. Olivier, J. P. Chopart, O. Aaboubi and G. Maurin, *J. Electrochem. Soc.*, 145 (1998) 401
28. O. Devos, O. Aaboubi, J. P. Chopart, E. Merienne, A. Olivier and J. Amblard, *J. Electrochem. Soc.*, 145 (1998) 4135
29. H. Matsushima, T. Nohira, I. Mogi and Y. Ito, *Surf. Coat. Technol.*, 179 (2004) 245
30. F. M. F. Rhen and J. M. D. Coey, *J. Phys. Chem. C*, 111 (2007) 3412
31. T. Iida, H. Matsushima and Y. Fukunaka, *J. Electrochem. Soc.*, 159 (2007) E112
32. D. Y. Li and J. A. Szpunar, *Electrochim. Acta*, 42 (1997) 47